iScience

CellPress
OPEN ACCESS

Article

SDG2 regulates Arabidopsis inflorescence architecture through SWR1-ERECTA signaling pathway

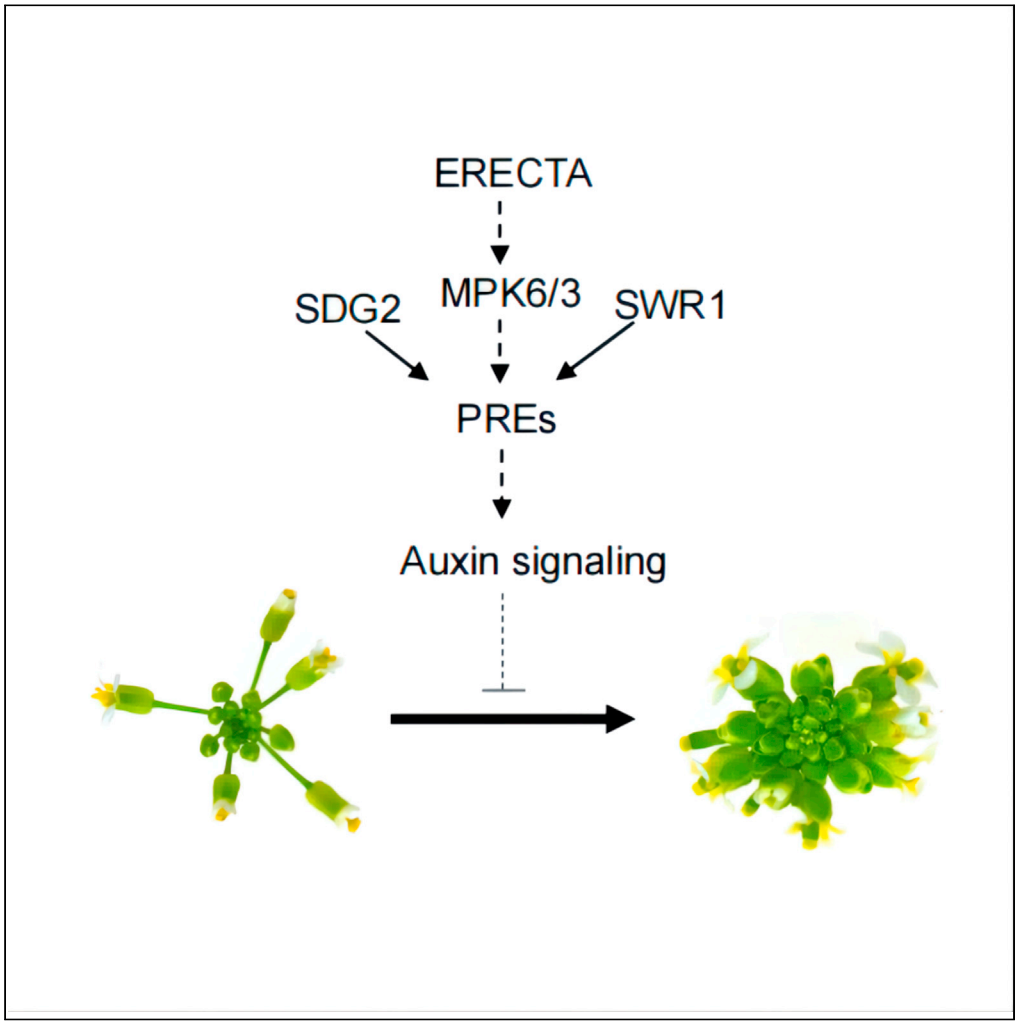

Liping Liu, Mengnan Chai, Youmei Huang, ..., Fangqian Chen, Yuan Qin, Hanyang Cai

caihanyang123@163.com

Highlights

SDG2 genetically interacts with the SWR1-ERECTA pathway in inflorescence development

SWR1-ERECTA pathway is required to enrich H2A.Z and H3K4me3 at auxin-related genes

H2A.Z histone variant enrichment was regulated by SDG2

Liu et al., iScience 24, 103236
November 19, 2021
https://doi.org/10.1016/j.isci.2021.103236

iScience

CellPress
OPEN ACCESS

Article

SDG2 regulates Arabidopsis inflorescence architecture through SWR1-ERECTA signaling pathway

Liping Liu,[1,3] Mengnan Chai,[1,3] Youmei Huang,[1,3] Jingang Qi,[1] Wenhui Zhu,[1] Xinpeng Xi,[1] Fangqian Chen,[1] Yuan Qin,[1,2] and Hanyang Cai[1,4,*]

SUMMARY

Inflorescence architecture is diverse in flowering plants, and two determinants of inflorescence architecture are the inflorescence meristem and pedicel length. Although the ERECTA (ER) signaling pathway, in coordination with the SWR1 chromatin remodeling complex, regulates inflorescence architecture with subsequent effects on pedicel elongation, the mechanism underlying *SWR1-ER* signaling pathway regulation of inflorescence architecture remains unclear. This study determined that SDG2 genetically interacts with the *SWR1-ER* signaling pathways in regulating inflorescence architecture. Transcriptome results showed that auxin might potentially influence inflorescence growth mediated by SDG2 and *SWR1-ER* pathways. SWR1 and ER signaling are required to enrich H2A.Z histone variant and SDG2 regulated SDG2-mediated H3K4me3 histone modification at auxin-related genes and H2A.Z histone variant enrichment. Our study shows how the regulation of inflorescence architecture is mediated by SDG2 and SWR1-ER, which affects auxin hormone signaling pathways.

INTRODUCTION

Inflorescence architecture is determined by the Spatio-temporal arrangement of flowers on a stem, which directly affects seed production and is complex and delicate. In recent years, much attention has been drawn to plant inflorescence architecture, which is a key element to improving crop yield and grain quality. The inflorescence architecture depends on its branching pattern and the position of the flowers, in other words, when and where flowers are formed (Benlloch et al., 2007). The appearance of each inflorescence type varies depending on the arrangement of lateral meristems around the stem (phyllotaxy), the pattern of internode lengths, and additional variations on the three architectural themes (Prusinkiewicz et al., 2007). In Arabidopsis, the shoot apical meristem (SAM) is a vegetative meristem that produces leaves and branches, is an open-raceme, where the flower formed from the flanks of the inflorescence SAM (Amasino and Michaels, 2010; Fernandez-Nohales et al., 2014; Huijser and Schmid, 2011).

Some genes involved in regulating plant inflorescence architecture have been reported in recent years. For example, *Jatropha ADENOSINE KINASE 2* (*JcADK2*), *ADENINE PHOSPHORIBOSYLTRANSFERASE 1* (*JcAPT1*) and *CYTOKININ OXIDASE 3* (*JcCKX3*) which control inflorescence branching in *Jatropha* by regulating cytokinin metabolic pathway (Chen et al., 2019a). *Panicle Morphology Mutant 1* (*PMM1*), a new allele of *DWARF11* (*D11*), was identified that might have potential roles in affecting the differentiation of spikelet primordia and patterns of panicle branches in rice through BRs biosynthesis (Li et al., 2018). The transcription factors encoded by *SQUAMOSA PROMOTER BINDING PROTEIN LIKE* (*SPL*) gene family and the *miR156-SPL* module regulate plant growth and architecture. In Arabidopsis, *miR156* regulated transcription factors *AtSPL3, AtSPL4,* and *AtSPL5* show a high sequence identity and promoted the floral meristem identity transition (Cui et al., 2020; Prusinkiewicz et al., 2007; Wu and Poethig, 2006; Xu et al., 2016). Furthermore, *miR156a* influences inflorescence architecture in tomatoes by suppressing the *SPL* transcription factor gene family (Zhang et al., 2011). Further investigation indicated that *SPL13* was the major *SPL* involved in *miR156a*-regulated tomato inflorescence architecture (Cui et al., 2020). A mitogen-activated protein kinase (MPK) cascade has previously been indicated to function downstream of the ER receptor in regulating localized cell proliferation in Arabidopsis (Meng et al., 2012). The evolutionarily conserved SWR1 complex plays a crucial role in several biological processes by catalyzing H2A.Z deposition in nucleosomes (Aslam et

[1]College of Life Science, Fujian Provincial Key Laboratory of Haixia Applied Plant Systems Biology, Fujian Agriculture and Forestry University, Fuzhou 350002, China

[2]State Key Laboratory for Conservation and Utilization of Subtropical Agro-Bioresources, Guangxi Key Lab of Sugarcane Biology, College of Agriculture, Guangxi University, Nanning 530004, China

[3]These authors contributed equally

[4]Lead contact

*Correspondence: caihanyang123@163.com

https://doi.org/10.1016/j.isci.2021.103236

al., 2019; Kumar, 2018). Our recent results showed that the basic helix-loop-helix (*bHLH*) transcription factor *PACLOBUTRAZOL RESISTANCE1* (*PRE1*) acts downstream of *ER-MPK* signaling cascade regulating inflorescence architecture. In addition, the ATP-dependent chromatin remodeling complex SWR1 plays a crucial role in controlling the *ER-MPK-PREs* signaling pathway (Cai et al., 2017). Genetic interactions between ER signaling and the chromatin remodeling complex SWR1 in the control of inflorescence architecture were studied (Cai et al., 2017). Further investigation showed that *HOMOLOG OF BEE2 INTERACTING WITH IBH1* (*HBI1*) functions downstream of the ER-MPK-PREs signaling pathway and regulates the inflorescence architecture via affecting the brassinosteroid (BR) biosynthesis and auxin signaling pathway (Cai et al., 2020). HBI1 directly binds to the promoters of the BR biosynthesis gene *CYP85A2* and a series of auxin-related genes including *ARF3* to promote their expression and regulate pedicel cortex cell proliferation and pedicel elongation. In turn, ARF3 can also bind to these auxin-related genes and *CYP85A2* and activate their expression, consistent with the role of ARF3 as a master regulator that establishes a feedback loop of auxin signaling. The findings also show how inflorescence architecture regulation mediated by the *SWR1-ER* pathways involves the HBI1 regulatory hub, which affects both the BR and auxin hormone signaling pathways (Cai et al., 2020).

Histone H3 lysine 4 trimethylation (H3K4me3) is a prominent histone methylation mark, acting as an active transcription mark in the epigenetic regulation of gene expression (Guo et al., 2010). The histone methylation is mediated by the histone lysine (K) methyltransferases (HKMTases) (Zhou et al., 2020), and many of HKMTases have been identified in plants and animals (Alvarez-Venegas and Avramova, 2002; Baumbusch et al., 2001; Guo et al., 2010; Springer et al., 2003; Zhao and Shen, 2004). Among these, HKMTases with a *SET* domain are called the SET domain group (SDG) proteins (Guo et al., 2010; Springer et al., 2003), and only SDG proteins can work as HKMTases in plants (Zhou et al., 2020). Functional studies of the *SDG* family in Arabidopsis, maize, and rice have shown that *SDG* genes are involved in multiple biological processes of plant development (Berr et al., 2009; Jiang et al., 2018; Liu et al., 2016, 2017; Springer et al., 2003; Zhao et al., 2005). For example, *SDG721* and *SDG705* encode TRITHORAX-like proteins, which appear to modulate H3K4 methylation levels. Loss of *SDG721* and *SDG705* function resulted in reduced panicle branching in rice (Jiang et al., 2018). *SDG2*, a member of a novel class of H3K4methyltransferases (Yun et al., 2012), has been reported to affected sporophyte and gametophyte development (Berr et al., 2010b) and is involved in the regulation of stem cell activity in Arabidopsis (Yao et al., 2013). Although the pleiotropic roles of *SDG2* in Arabidopsis development are known, *SDG2* function in the regulation of inflorescence architecture has remained largely unclear. In recent years it has been shown that H2A.Z deposition and histone methylation affects gene expression in a genome-wide manner in different organisms (Dai et al., 2018; Hu et al., 2013). Our previous data showed that the accumulation of anthocyanin in H2A.Z deposition-deficient mutants is associated with increased H3K4me3. This data revealed an antagonistic relationship between H2A.Z deposition and H3K4me3 in regulating the expression of anthocyanin biosynthesis genes. However, little is known about the roles of these two types of epigenetic regulation marks in the control of inflorescence architecture.

This study shows that *SDG2* genetically interacts with the *SWR1* and *ER-MPK6-PREs* pathways in regulating inflorescence architecture. Furthermore, transcriptome data indicate that auxin may potentially influence inflorescence growth mediated by *SDG2* and *SWR1-ER-PREs*. *SWR1* and *ER* signaling are required to enrich the H2A.Z histone variant and *SDG2*-mediated H3K4me3 histone modification at auxin-related genes. SDG2 also regulated enrichment of the H2A.Z histone variant. Our study reveals how H2A.Z, H3K4me3, and *ER* signaling mutually regulate inflorescence architecture by affecting auxin hormone signaling pathways.

RESULTS

SDG2 is involved in the *SWR1* and *ER* signaling pathway in regulating inflorescence architecture

Previously we showed that the H3K4me3 level of *PRE1* was altered in *arp6 er-119* (Cai et al., 2017), and H2A.Z can coordinate with H3K4me3 to regulate gene's expression (Cai et al., 2020; Dai et al., 2018). *arp6* is a knockout line of *Actin related protein 6* (*ARP6*) that encodes a subunit of SWR1 complex (Choi et al., 2005). To test if H3K4me3 also regulates inflorescence architecture, we first examined the inflorescence architecture of *sdg2*. SDG2 is a coenzyme that mediates H3K4me3 in Arabidopsis and *sdg2* displays severely reduced H3K4me3 levels (Guo et al., 2010). *sdg2* mutants show clustered inflorescence architecture phenotype (Figure 1A) is associated with a reduced pedicel length (Figures 1B–1D) and reduced cortex

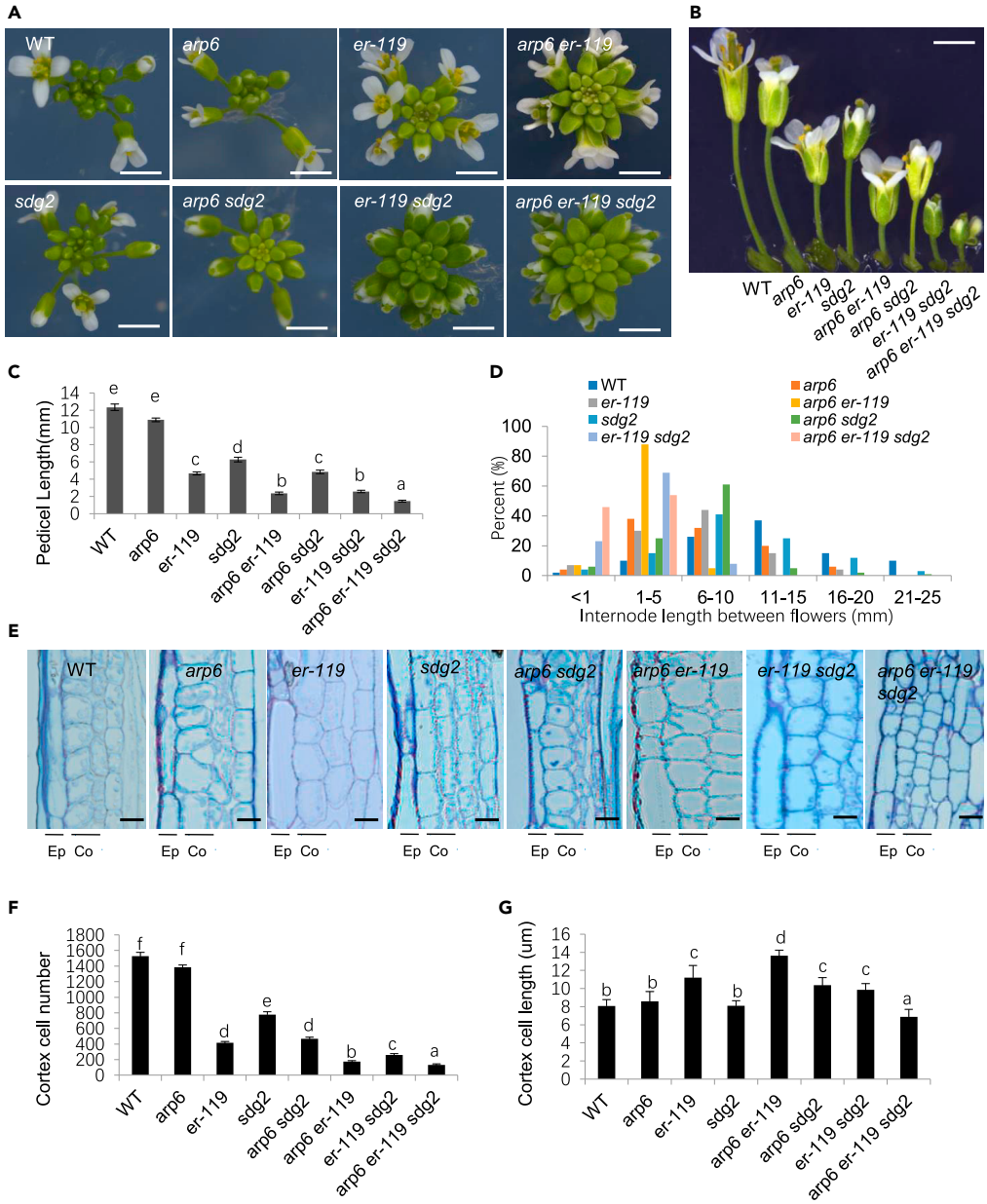

Figure 1. *SDG2* involvement in the regulation of inflorescence architecture and pedicel elongation in Arabidopsis

(A) Inflorescence stems apices of WT, *arp6*, *er-119*, *arp6 er-119*, *sdg2*, *arp6 adg2*, *er-119 sdg2*, and *arp6 er-119 sdg2* plants. Bars, 5mm. Fully open mature flowers and attached pedicels of the indicated genotype. Bar,10mm.

(B) Lengths of mature pedicels of fully open flowers from the main stems of 4-to5-wk-old plants. Bars represent average values ±SD (n = 10 pedicels per genotype). Different letters above columns indicate significant difference at $p < 0.05$, as determined by one-way ANOVA.

(C) Distribution of the internode length between two successive siliques. Ten internodes between the 1st and 11th siliques were analyzed for 10 pedicels per genotype.

(D) Longitudinal sections of mature pedicels from fully open flowers of WT, *arp6*, *er-119*, *arp6 er-119*, *sdg2*, *arp6 adg2*, *er-119 sdg2*, and *arp6 er-119 sdg2* plants. Co, cortex; Ep, epidermis. Bars, 10μm.

(E) Cell numbers in the longitudinal cortex file of mature pedicels from fully open flowers (n = 10 pedicels per genotype). Different letters above columns indicate significant difference at $p < 0.05$, as determined by one-way ANOVA.

(F) Quantitative analysis of cortex cell length. Bars represent average values ± SD (n = 10 pedicels per genotype).

(G) Quantitative analysis of cortex cell length. Bars represent average values ±SD (n = 10 pedicels per genotype). Different letters above columns indicate significant difference at $p < 0.05$, as determined by one-way ANOVA.

cell numbers compared with WT (Figures 1E and 1F). The cortex cell length in *sdg2* mutant is comparable to WT (Figure 1G). These phenotypes are similar to those described for mutants of the *SWR1-ER* signaling pathway, which exhibited reduced pedicel length caused by defective cell proliferation in the pedicel cortex (Cai et al., 2017). We next crossed *sdg2* with *arp6*, *er-119* single and *arp6 er-119* double mutants. *arp6 sdg2*, *er-119 sdg2* double mutants showed significantly enhanced compact inflorescence architecture compared to *arp6* and *er-119* single mutants, respectively (Figure 1). In addition, *arp6 er-119 sdg2* triple mutants showed significantly enhanced compact inflorescence architecture compared to *arp6 er-119* double mutant (Figure 1). The compact inflorescence architecture in *arp6 sdg2*, *er-119 sdg2* double mutants and *arp6 er-119 sdg2* triple mutants were associated with short pedicel lengths (Figures 1B–1D), reduced pedicel cell number in the cortex and the pedicel epidermal cell length compared to WT, *arp6*, *er-119*, and *sdg2* mutants, respectively (Figures 1E and 1F; S1). To investigate whether *SDG2* acts downstream of *SWR1-ER* regulating inflorescence architecture, we crossed *pSDG2:myc-SDG2* into *arp6 er-119*. In the F_2 generation, individual *arp6 er-119* plants carrying the *pSDG2:myc-SDG2* transgene were obtained and all exhibited a partially rescued compact inflorescence (Figure 2A). The defect pedicel length could be partially rescued compared to *arp6 er-119* (Figures 2B–2D) accompanied with significantly increased pedicel cortex cell number (Figures 2E–2G). These data suggested that *SDG2* is involved in SWR1 and ER-dependent regulation of inflorescence architecture.

SDG2 is involved in the *PREs*-controlled inflorescence architecture

Previous studies have demonstrated that *PREs* transcription factors are involved in flower development and petiole/hypocotyl elongation in Arabidopsis (Shin et al., 2019). However, little is known about *SDG2* and its effect on inflorescence architecture in Arabidopsis. Our data indicate that *SDG2* is involved in *SWR1-ER* signaling pathway regulating inflorescence architecture (Figures 1 and 2). Our previous results have shown *PREs* shared overlapping functions downstream of *SWR1-ER* in regulating inflorescence architecture (Cai et al., 2017). Previous studies showed that the levels of H3K4me3 was a severe decrease in *sdg2* mutant, and the *PRE1* expression level was also a severe decrease in *sdg2* mutant compared to WT (Guo et al., 2010). To determine whether the levels of H3K4me3 were regulated by *SDG2* and *SWR1-ER* pathway, we assessed the levels of H3K4me3 by Western blotting using proteins extracted from WT, *sdg2*, and *arp6 er-119 sdg2* floral buds. The analysis revealed a severe decrease in the cellular level of H3K4me3 in *sdg2* single mutant and a more severe decrease in *arp6 er-119 sdg2* triple mutant (Figure 3A). The enrichment of H3K4me3 in *PREs* transcription start site (TSS) was significantly reduced in *er-119* and *sdg2* and reduced even further in *er-119 sdg2*, *arp6 er-119*, *arp6 sdg2* and *arp6 er-119 sdg2* compared to WT and *arp6* (Figure 3B). These results indicated that SDG2-mediated H3K4me3 was regulated by the *SWR1-ER* pathway and *PREs* were activated by *SWR1-ER* and *SDG2* pathway. To investigate whether *SDG2* also interacts genetically with *PREs* in regulating inflorescence architecture, we first performed qRT-PCR to compare *PREs* transcript levels in WT, *arp6*, *er-119*, *sdg2*, *er-119 sdg2*, *arp6 er-119*, *arp6 sdg2*, and *arp6 er-119 sdg2* mutants. The *PREs* levels were significantly reduced in *er-119* and *sdg2* and reduced even further in *er-119 sdg2*, *arp6 er-119*, *arp6 sdg2*, and *arp6 er-119 sdg2* compared to WT and *arp6* (Figure 3C). Next, we crossed *sdg2-1* with *pre-amiR*. Similar to *er-119 sdg2* and *arp6 er-119 sdg2* plants, the *sdg2 pre-amiR* mutant showed further reduced pedicels and internode lengths and more compact inflorescences than the *sdg2* and *pre-amiR* single mutants (Figures 4A–4D), reduced pedicel cell number in the cortex and the pedicel epidermal cell length (Figures 4E–4G and S1). Taken together, these results suggest that *SDG2* interacts genetically with *PREs* in regulating inflorescence architecture by promoting cell proliferation in the pedicel.

Transcriptome data reveals potential roles of phytohormones in inflorescence growth mediated by the *SWR1-SDG2-PREs* pathway

To further explore the potential mechanism of inflorescence growth regulated by *SWR1-SDG2-PREs* pathway, we analyze transcriptome data of WT, *arp6 sdg2*, *pre-amiR* inflorescence by RNA-seq, and the results showed that there were 448 commonly down-regulated and 98 commonly up-regulated genes in *arp6 sdg2* and *pre-amiR* compared to WT (Figures 5A and 5B). Gene ontology (GO) enrichment analysis showed that the down-regulated genes in *arp6 sdg2* and *pre-amiR* compared to WT were enriched in chemical stimulus, abiotic stimulus, organic substance and hormone stimulus (Figure 5C). The upregulated genes in *arp6 sdg2* and *pre-amiR* compared to WT were enriched in metabolic and biosynthetic processes (Figure 5D). Previous research supports that phytohormones are linked to plant development, particularly concerning pedicel elongation and inflorescences architecture. We previously demonstrated that auxin plays a role in inflorescence growth mediated by *SWR1-ER-PREs* signaling pathway (Cai et al., 2017,

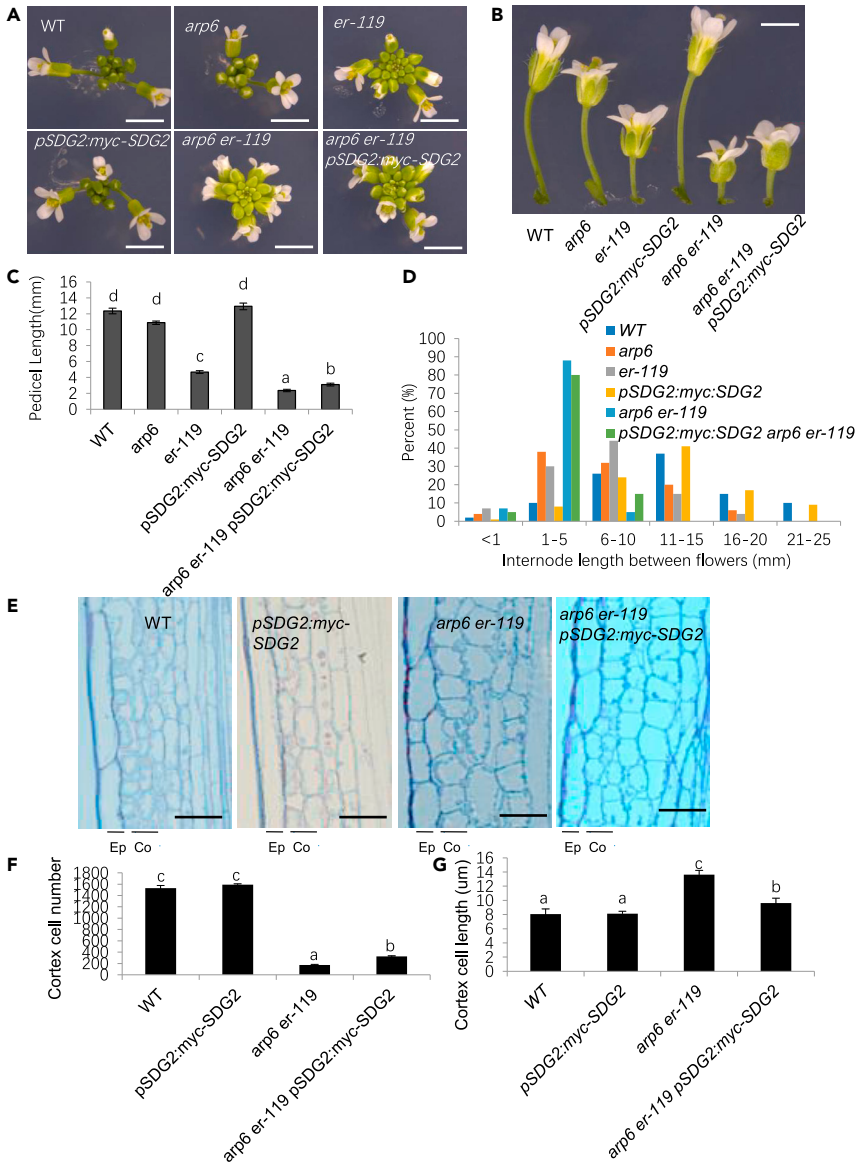

Figure 2. *SDG2* is involved in *SWR1-ER* signaling pathway in regulating inflorescence architecture

(A) Inflorescence stem apices of WT, *arp6*, *er-119*, *pSDG2:myc-SDG2*,*arp6 er-119*, and *arp6 er-119 pSDG2:myc-SDG2* plants. Bars, 5mm.

(B) Fully open mature flowers and attached pedicels of the indicated genotype. Bar,10mm.

(C) Lengths of mature pedicels of fully open flowers from the main stems of 4-to5-wk-old plants. Bars represent average values ±SD (n = 10 pedicels per genotype). Different letters above columns indicate significant difference at $p < 0.05$, as determined by one-way ANOVA.

(D) Distribution of the internode length between two successive siliques. Ten internodes between the 1st and 11th siliques were analyzed for 10 pedicels per genotype.

(E) Longitudinal sections of mature pedicels from fully open flowers of WT, *pSDG2:myc-SDG2*,*arp6 er-119*, and *arp6 er-119 pSDG2:myc-SDG2* plants. Co, cortex; Ep, epidermis. Bars, 10μm.

(F) Cell numbers in the longitudinal cortex file of mature pedicels from fully open flowers (n = 10 pedicels per genotype). Different letters above columns indicate significant difference at $p < 0.05$, as determined by one-way ANOVA.

(G) Quantitative analysis of cortex cell length. Bars represent average values ± SD (n = 10 pedicels per genotype). Different letters above columns indicate significant difference at $p < 0.05$, as determined by one-way ANOVA.

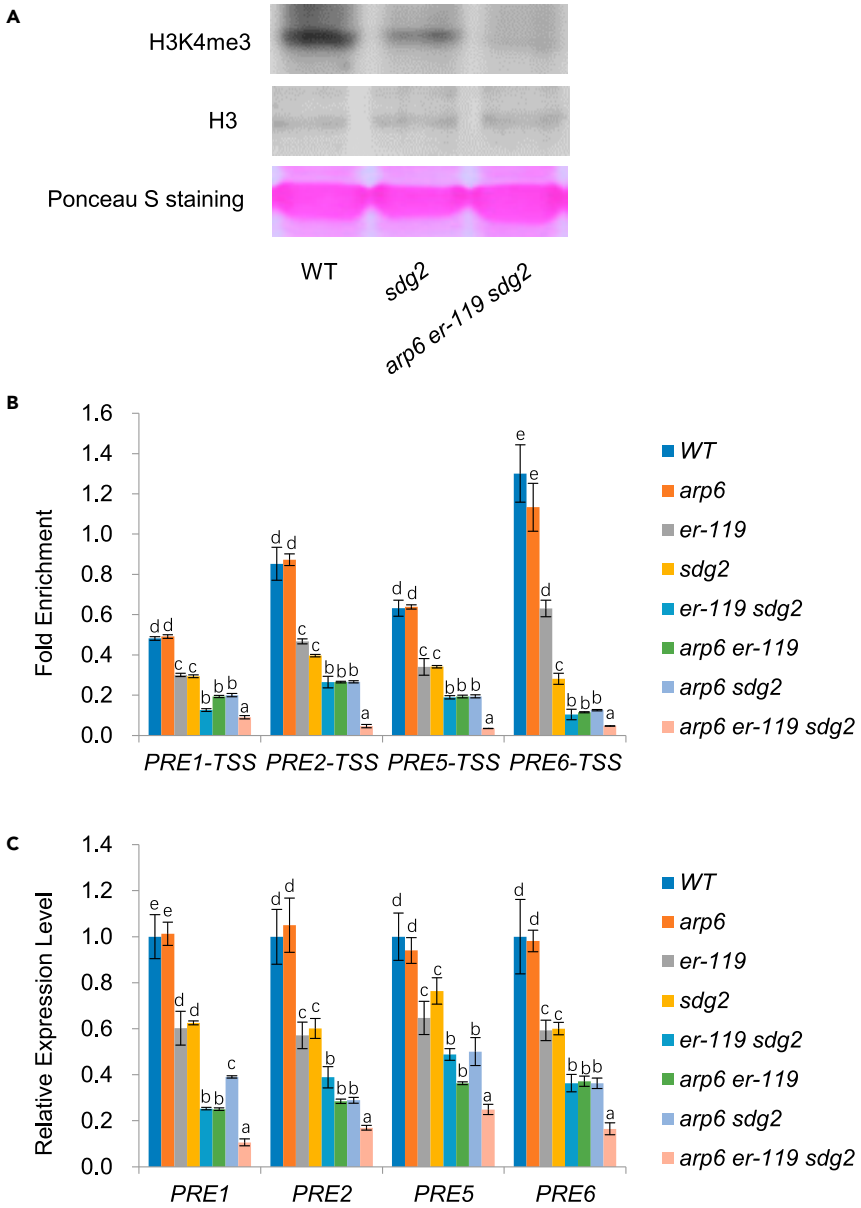

Figure 3. H3K4me3 level is severely reduced in *sdg2* and *arp6 er-119 sdg2*

(A) Western blot analysis of the cellular level of H3K4me3 in WT, *sdg2*, and *arp6 er-119 sdg2*. For each modification, the same membrane was stripped and blotted with an antibody against H3. Ponceau S staining indicates that the protein samples are consistent.

(B) ChIP analysis for the enrichment of H3K4me3 at *PRE1,2,5,6* TSS (transcription start site) region in WT, *arp6*, *er-119*, *sdg2*, *er-119 sdg2*, *arp6 er-119*, *arp6 sdg2*, and *arp6 er-119 sdg2* flower buds. Different letters above columns indicate significant difference at $p < 0.05$, as determined by one-way ANOVA.

(C) The expression of *PRE1,2,5,6* is down-regulated in *Arabidopsis er-119*, *sdg2*, *er-119 sdg2*, *arp6 er-119*, *arp6 sdg2*, and *arp6 er-119 sdg2* floral buds. Different letters above columns indicate significant difference at $p < 0.05$, as determined by one-way ANOVA.

2020). Considering the enrichment of hormone-regulated genes among the down-regulated genes, we generated an expression heatmap of these genes in *arp6 sdg2* and *pre-amiR* compared to WT. Auxin-related genes with significantly reduced *arp6 sdg2 and pre-amiR* mutants include auxin-induced *SAURs*, *ARGOS*, auxin influx carrier *IAAs*, auxin efflux carriers *PIN3*, and auxin transporter *PILS5*, and GA-/BR- regulated genes (Figure 5E). To verify the transcriptome, we performed qRT-PCR analysis and could verify the

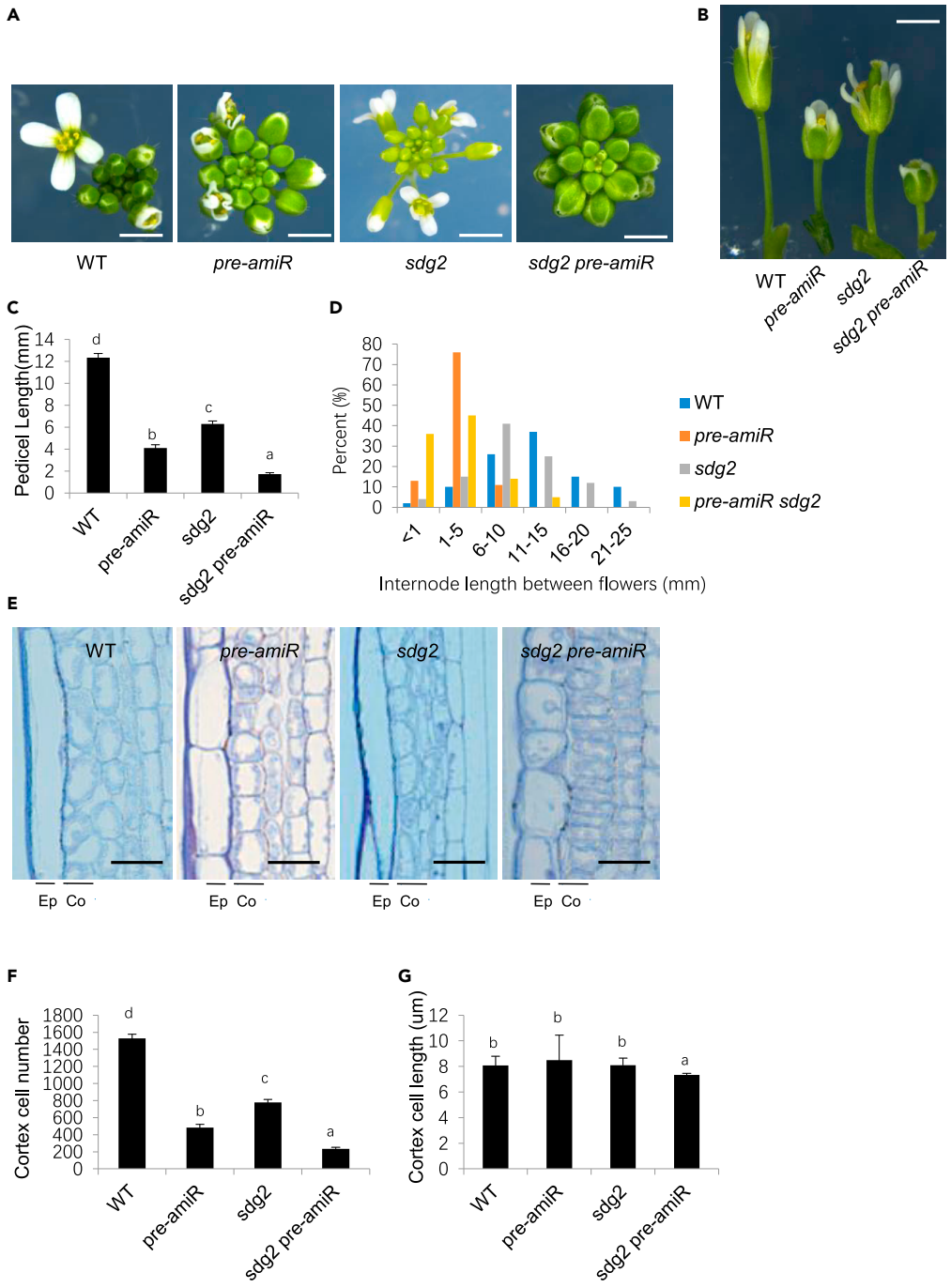

Figure 4. *SDG2* is involved in the *PREs*-controlled inflorescence architecture

(A) Inflorescence stems apices of WT, *pre-amiR*, *sdg2*, *sdg2 pre-amiR* plants. Bars, 5 mm.

(B) Fully open mature flowers and attached pedicels of the indicated genotype. Bar, 10 mm.

(C) Lengths of mature pedicels of fully open flowers from the main stems of 4-to5-week-old plants. Bars represent average values ±SD (n = 10 pedicels per genotype). Different letters above columns indicate significant difference at $p < 0.05$, as determined by one-way ANOVA.

(D) Distribution of the internode length between two successive siliques. Ten internodes between the 1st and 11th siliques were analyzed for 10 pedicels per genotype.

(E) Longitudinal sections of mature pedicels from fully open flowers of WT, *pre-amiR*, *sdg2*, *sdg2 pre-amiR* plants. Co, cortex; Ep, epidermis. Bars, 10μm.

Figure 4. *Continued*
(F) Cell numbers in the longitudinal cortex file of mature pedicels from fully open flowers (n = 10 pedicels per genotype). Different letters above columns indicate significant difference at $p < 0.05$, as determined by one-way ANOVA.
(G) Quantitative analysis of cortex cell length. Bars represent average values ± SD (n = 10 pedicels per genotype). Different letters above columns indicate significant difference at $p < 0.05$, as determined by one-way ANOVA.

down regulation of those tested genes in *arp6 sdg2* and *pre-amiR* compared to WT, including *PIN3*, *PIL5*, *SAUR66*, *IAA14*, *GH3.17*, *IAA19*, *EXPA1*, and *ARL* (Figure 5F). These results suggested that the *SWR1-SDG2-PREs* pathway controls inflorescence architecture by regulating the expression levels of phytohormone-related genes, such as auxin-related genes.

H2A.Z deposition at auxin-related genes were altered in *arp6 er-119*, *arp6 sdg2* and *arp6 er-119 sdg2*

H2A.Z deposition has a conserved role in the various cellular processes through its function in chromatin structure and dynamics in eukaryotes (Kumar, 2018). The replacement of H2A by H2A.Z in nucleosomes depends on ATP-dependent chromatin remodeling complex SWR1 (Mizuguchi et al., 2004). In preceding results, we found that the relative expression level of auxin-related genes was significantly decreased in *arp6 sdg2* and *pre-amiR* compared to WT. To further clarify how H2A.Z deposition affects *SDG2* function in inflorescence architecture via *SWR1-SDG2-PREs* signaling pathway. We performed chromatin immunoprecipitation (ChIP) experiment using an H2A.Z antibody of WT, *arp6*, *sdg2*, *er-119*, *er-119 sdg2*, *arp6 er-119*, *arp6 sdg2*, and *arp6 er-119 sdg2* floral buds. We detected an enrichment of H2A.Z in the region of TSS and the ±1 nucleosome of auxin-related genes. The results showed that the enrichment of H2A.Z in the region of TSS and ±1 nucleosome of *PIN3*, *PIL5*, *SAUR66*, *IAA14*, *GH3.17*, *IAA19*, *EXPA1*, and *ARL* was significantly decreased in *arp6* mutant and was further depleted in *arp6 er-119*, *arp6 sdg2* double mutants, and *arp6 er-119 sdg2* triple mutant compared with *arp6* mutant and WT. No decrease of H2A.Z deposition in the region of TSS and ±1 nucleosome could be detected in *sdg2*, *er-119*, and *er-119 sdg2* mutants (Figures 6A–6H). These results indicated that the deposition of H2A.Z on auxin-related gene loci depends on *ARP6* but not *ER or SDG2*. In Arabidopsis, *AT4G07700* is widely believed to contain H2A.Z-free nucleosomes. To confirm whether the lack of H2A.Z signal in these assays corresponds with the absence of H2A.Z, we detected the H2A.Z deposition in *AT4G07700*. In WT and mutants, the deposition of H2A.Z was not detected in all assayed regions of *AT4G07700* (Figure 6I). In addition, we also detected H2A.Z deposition in TSS and ±1 nucleosome regions of *AtHSP70*, which is known as H2A.Z positive control gene, and found a decrease of H2A.Z in *arp6*, *arp6 er-119* and *arp6 sdg2* floral buds compare with WT (Figure 6J).To ensure the accuracy of ChIP-qPCR assays by using H2A.Z antibody, we further sequence the ChIP-qPCR products. The results showed that the sequences of the ChIP-qPCR products were the same as the expected sequences (Figure S2). These indicated that the ChIP-qPCR used is accurate.

The Pol II, H3K4me3 and H3K27me3 levels of auxin-related genes were altered in *arp6 er-119*, *er-119 sdg2*, *arp6 sdg2* and *arp6 er-119 sdg2*

Polymerase II (Pol II) is required for active transcription, and previous research indicated that Pol II enrichment was widely affected by H2A.Z deposition (Dai et al., 2018). Next, we wanted to analyze if the detected the decrease of H2A.Z deposition in *arp6 er-119*, *er-119 sdg2*, and *arp6 sdg2* double mutants and *arp6 er-119 sdg2* triple mutant leads to an enrich Pol II association in those genes. We performed a ChIP assay using a Pol II antibody. Pol II enrichment was not altered at *PIN3*, *PIL5*, *SAUR66*, *IAA14*, *GH3.17*, *IAA19*, *EXPA1*, and *ARL* in *arp6* and *sdg2* mutants compared to WT (Figure 7). However, the Pol II enrichment was significantly reduced at *PIN3*, *PIL5*, *SAUR66*, *IAA14*, *GH3.17*, *IAA19*, *EXPA1*, and *ARL* in the *er-119* single mutant, *arp6 er-119* and *arp6 sdg2* double mutants, and the Pol II enrichment was more significantly reduced at *PIN3*, *PIL5*, *SAUR66*, *IAA14*, *GH3.17*, *IAA19*, *EXPA1*, and *ARL* in *arp6 er-119 sdg2* triple mutant compared to WT, *arp6* and *sdg2* single mutants (Figure 7). To ensure the accuracy of ChIP-qPCR assays by using Pol II antibody, we further sequence the ChIP-qPCR products. The results showed that the sequences of the ChIP-qPCR products were the same as expected sequences (Figure S2). These indicated that the ChIP-qPCR results are reliable.

Histone methylation plays a broad and important role in transcription regulation. Actively transcribed genes contain H3K4me3, whereas developmentally repressed genes are enriched for H3K27me3 (Berr et al., 2010a, 2010b; Li et al., 2013). H2A.Z is widely known to mediate the different histone modifications through affecting the *MLL* and *PRC2* complex activity (Hu et al., 2013). To investigate the transcriptional

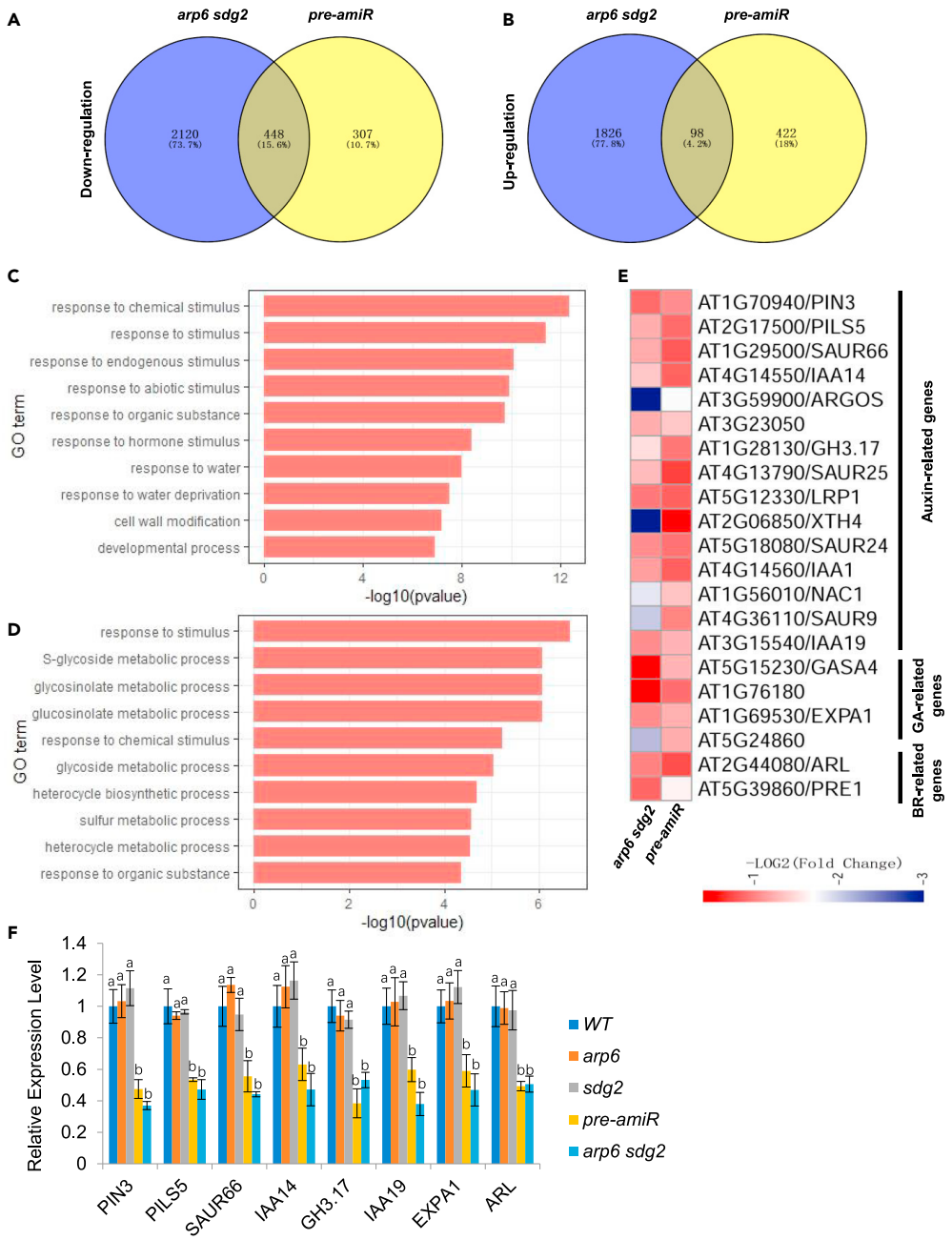

Figure 5. Gene expression profiling of *arp6 sdg2* and *pre-amiR* inflorescences compared WT revealed a set of commonly regulated genes

(A and B) Venn diagrams show the number of downregulated and upregulated. Genes in both *arp6 sdg2* and *pre-amiR* compared with WT.

(C and D) The top 10 Gene Ontology (GO) terms (ranked by p value) for the commonly regulated genes. Downregulated and upregulated genes in both *arp6 sdg2* and *pre-amiR* compared with WT.

(E) Heatmap showing the down regulation of the indicated genes in *arp6 sdg2* and *pre-amiR* compared with WT. from RNA-sequencing analysis. The average of three replicates is shown to demonstrate consistency. The scale represents log10-transformed expression values, and the genes are grouped according to functional classification. FPKM, fragments per kilobase of exon model per million reads mapped.

(F) Quantitative real-time PCR expression analysis of auxin-related genes in pedicel tissues of WT and *arp6*, *sdg2*, *pre-amiR*, and *arp6 sdg2* mutants. Values are means ± SD from three biological replicates. Each biological replicate represents three technical repeats. Different letters above the columns indicate significant differences at $p < 0.05$, as determined by one-way ANOVA.

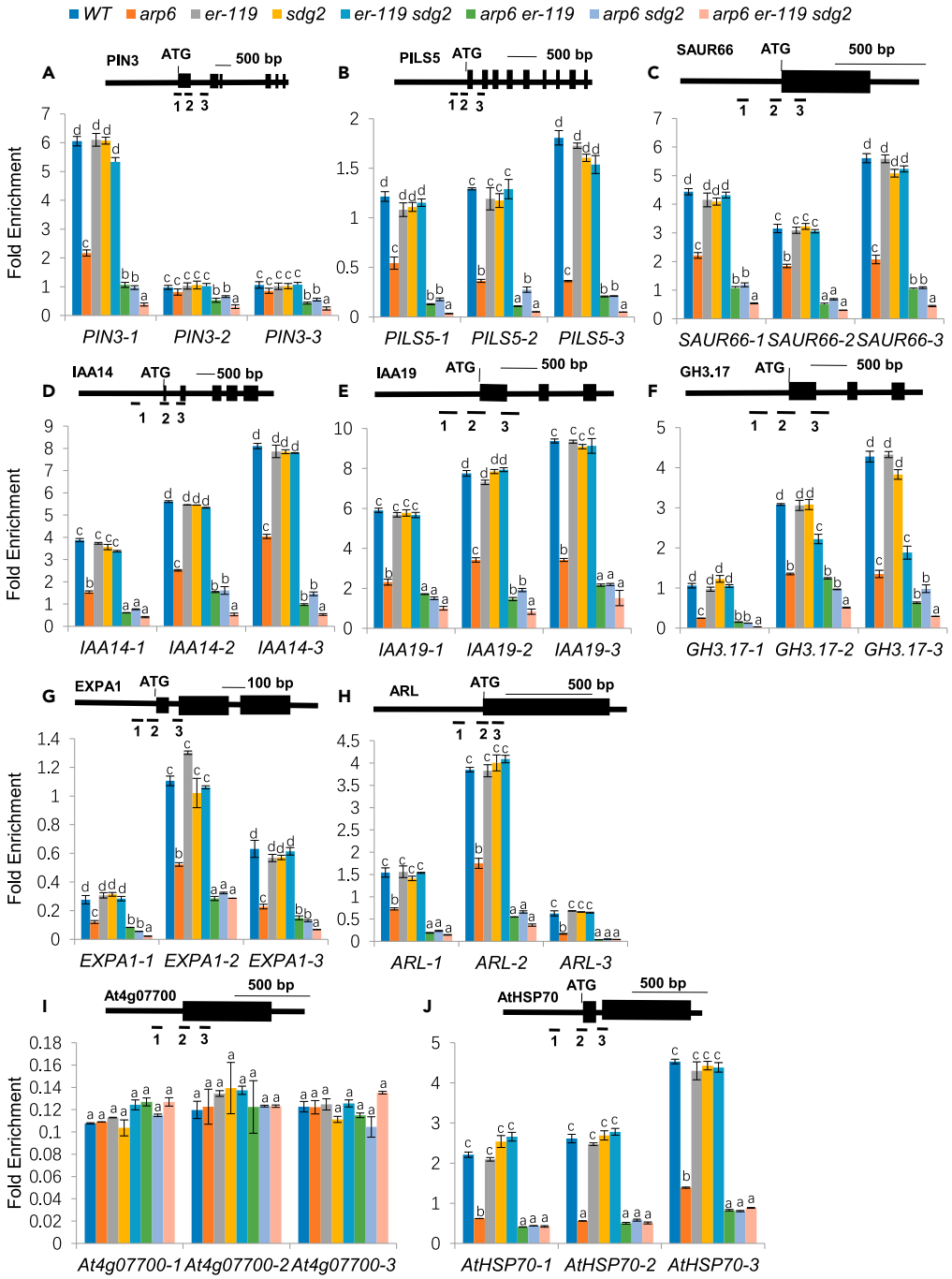

Figure 6. H2A.Z deposition at auxin-related genes were altered in *arp6 er-119*, *arp6 sdg2*, and *arp6 er-119 sdg2*.

(A–J) Diagram of *PIN3*, *PILS5*, *SAUR66*, *IAA14*, IAA*19*, *GH3.17*, *EXPA1*, *ARL*, *At4g07700*, and *AtHSP70* genes with exons indicated as black boxes and the promoter indicated as the region before ATG indicator. The transcription start site (TSS) is shown as a black indicator line. PCR primer sets are shown as black bars below the diagram. Primer set numbers to correspond to the numbers on the x axis of the graphs in Figures 5, 6, 7, 8, and 9. Different letters above columns indicate significant differences at were $p < 0.05$, as determined by one-way ANOVA.

regulation of auxin-related genes via H3K4me3 or H3K27me3 Histone methylation in *SWR1-SDG2-PRE1* signaling pathway, we detected the enrichment of H3K4me3 active maker and H3K27me3 repressive maker in auxin-related genes in WT, *arp6*, *er-119*, and *sdg2* single mutants, *er-119 sdg2*, *arp6 er-119*, and *arp6 sdg2* double mutants and *arp6 er-119 sdg2* triple mutant through using ChIP assays. The results showed

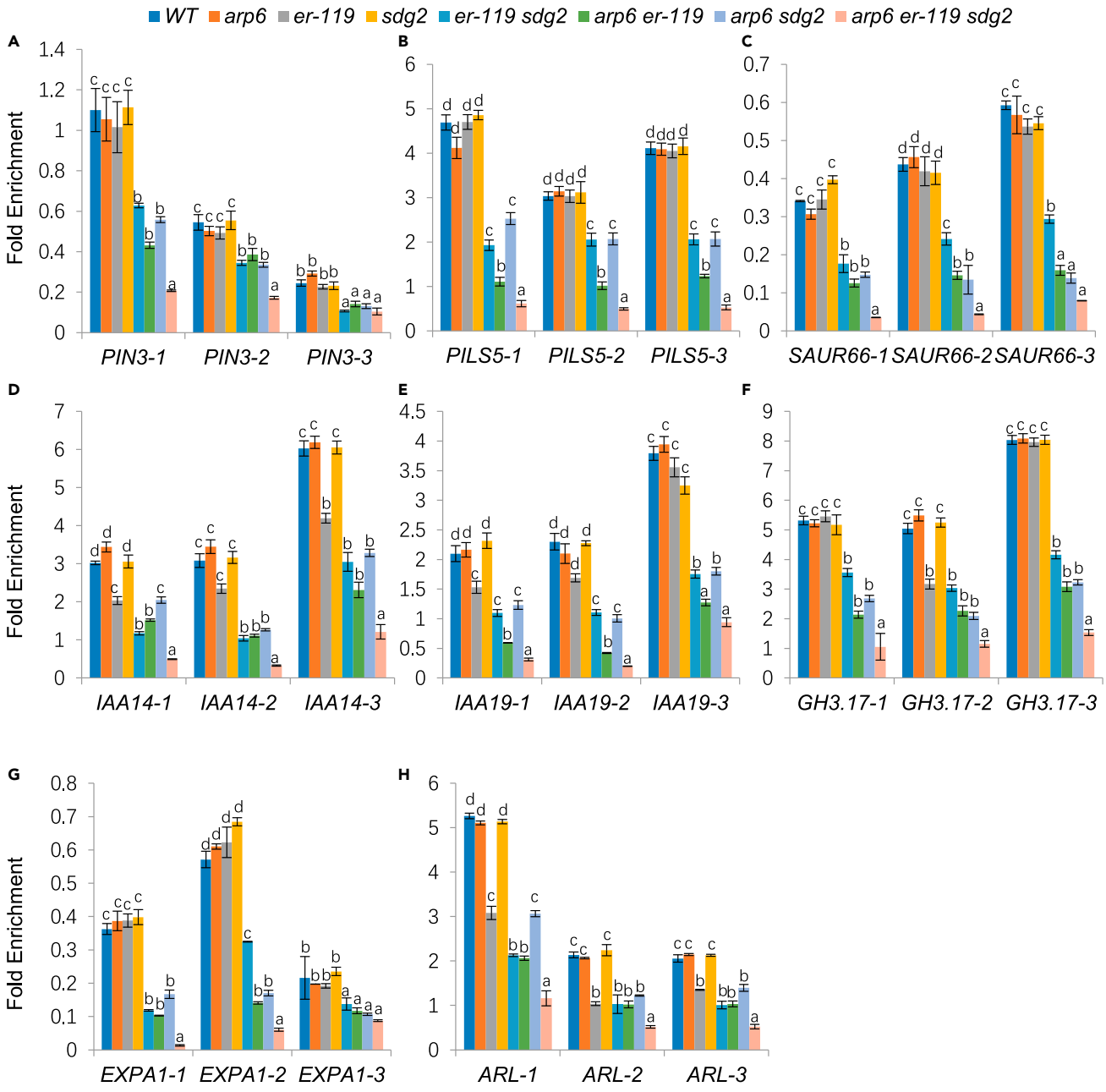

Figure 7. The Pol II level at auxin-related genes were altered in *arp6 er-119*, *arp6 sdg2*, and *arp6 er-119 sdg2*

(A–H) ChIP analysis for the enrichment of Pol II at auxin-related genes in WT, *arp6*, *er-119*, *sdg2*, *er-119 sdg2*, *arp6 er-119*, and *arp6 sdg2* flower buds. Different letters above columns indicate significant difference at $p < 0.05$, as determined by one-way ANOVA.

that H3K4me3 enrichment in most of the auxin-related genes was significantly decreased in *sdg2* single mutant and *er-119 sdg2*, *arp6 er-119*, and *arp6 sdg2* double mutants, and *arp6 er-119 sdg2* triple mutant compared with WT, *arp6* and *er-119* single mutants (Figure 8). In contrast to the performance of H3K4me3 reduced enrichment, a significantly increased enrichment of H3K27me3 in the region of TSS and ±1 nucleosome of these auxin-related genes was detected in *er-119 sdg2*, *arp6 er-119* and *arp6 sdg2* double mutants compared to WT, *arp6*, *sdg2* and *er-119* single mutants (Figure 9) and a more significantly increased enrichment of H3K27me3 in the region of TSS and ±1 nucleosome of these auxin-related genes was detected in *arp6 er-119 sdg2* triple mutant compared to *arp6 er-119*, *er-119 sdg2*, and *arp6 sdg2* double mutants (Figure 9). These results indicated that the reduced expression level of auxin-related genes in *er-119*

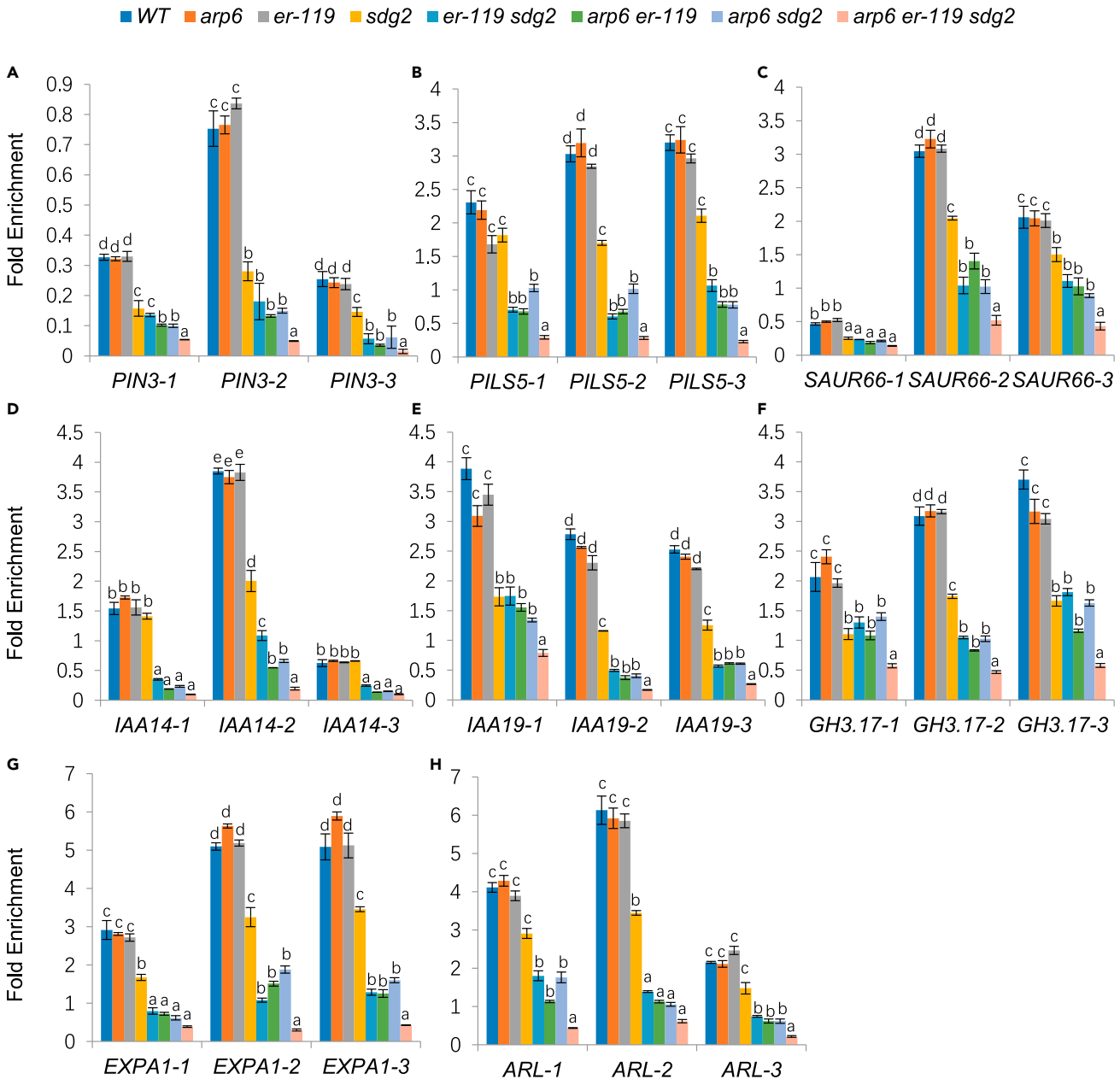

Figure 8. The H3K4me3 level at auxin-related genes were altered in *arp6 er-119*, *arp6 sdg2*, and *arp6 er-119 sdg2*

(A–H) ChIP analysis for the enrichment of H3K4me3 at auxin-related genes in WT, *arp6*, *er-119*, *sdg2*, *er119 sdg2*, *arp6 er-119*, and *arp6 sdg2* flower buds. Different letters above columns indicate significant difference at $p < 0.05$, as determined by one-way ANOVA.

sdg2, *arp6 er-119*, and *arp6 sdg2* double mutants and *arp6 er-119 sdg2* triple mutant compared to WT, *arp6*, *sdg2*, and *er-119* single mutants were correlated with the decreased enrichment of activation maker H3K4me3and the increased enrichment of repression maker H3K27me3 in auxin-related genes. To ensure the accuracy of ChIP-qPCR assays by using H3K4me3 and H3K27me3 antibodies, we further sequence the ChIP-qPCR products. The results showed that the sequences of the ChIP-qPCR products were the same as expected sequences (Figure S2). These indicated that the ChIP-qPCR results are reliable.

SDG2 binds to auxin-related genes are involved in *SWR1-ER* signaling pathway

We previously showed that the *SDG2* mediated H3K4me3 influences inflorescence architecture by interfering with the *SWR1-ER* signaling pathway. To further investigate whether SDG2 binding to auxin-related genes is

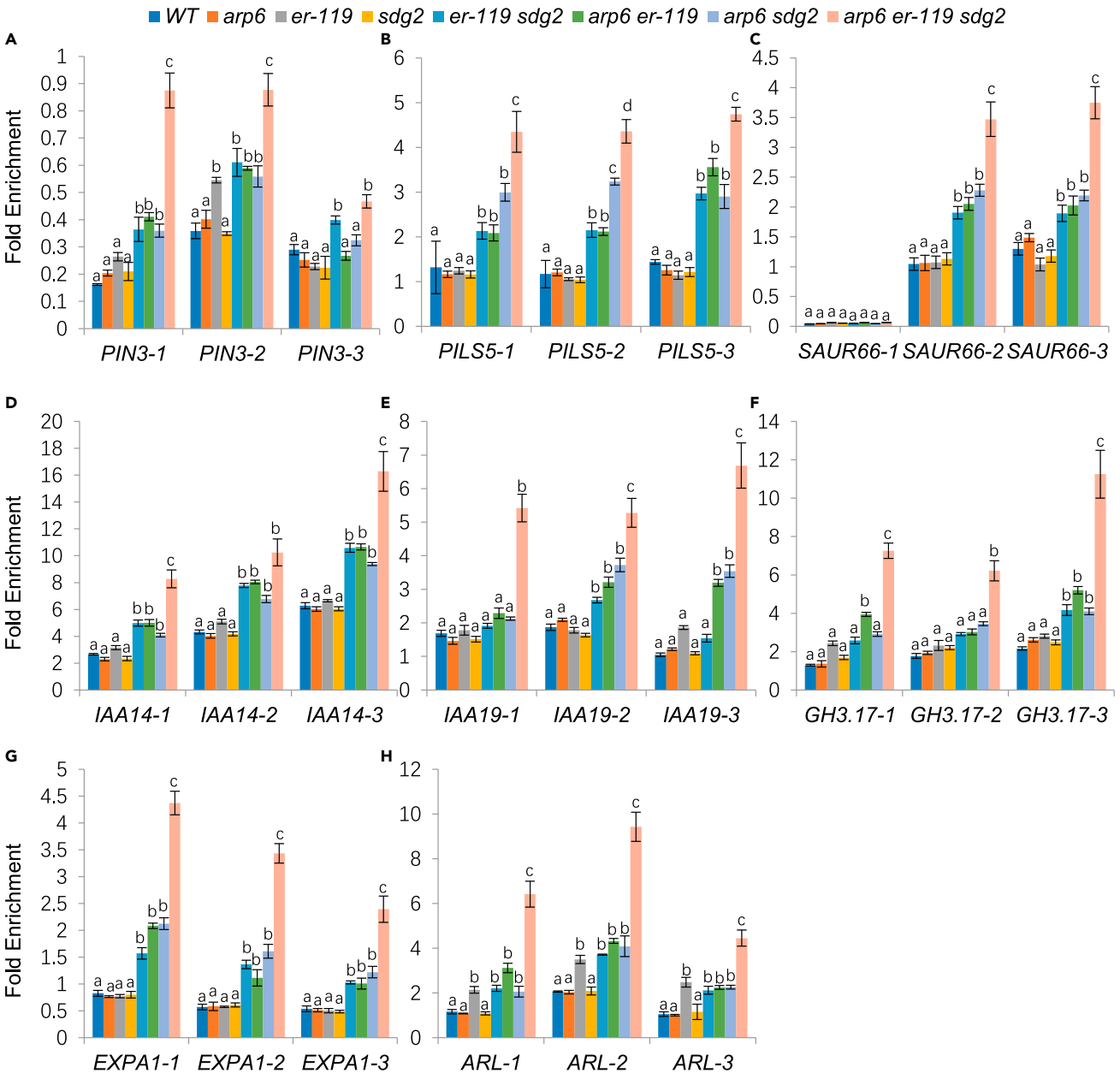

Figure 9. The H3K27me3 level at auxin-related genes were altered in *arp6 er-119*, *arp6 sdg2*, and *arp6 er-119 sdg2*

(A–H) ChIP analysis for the enrichment of H3K27me3 at auxin-related genes in WT, *arp6*, *er-119*, *sdg2*, *er-119 sdg2*, *arp6 er-119*, and *arp6 sdg2* flower buds. Different letters above columns indicate significant difference at $p < 0.05$, as determined by one-way ANOVA.

dependent on the SWR1- ER signaling pathway, we expressed *pSDG2: myc-SDG2* in *arp6 er-119* and wild type plants and performed ChIP-qPCR experiments using an anti-myc antibody. We found that SDG2 binds to the promoter and gene body regions of auxin-related genes which were significantly reduced in *arp6 er-119* (Figure 10). These results support further that *SDG2* and *SWR1-ER* signaling pathway regulates the expression of auxin-related genes and that the binding of *SDG2* to the auxin-related genes depends on the SWR1-ER signaling pathway.

DISCUSSION

SDG2 coordinates with *SWR1-ER* signaling pathway in regulating inflorescence architecture

The histone lysine methyltransferase domain containing *SDG2* was reported to be broadly expressed during plant growth (Guo et al., 2010) and mutants displayed defects in sporophytic and gametophytic

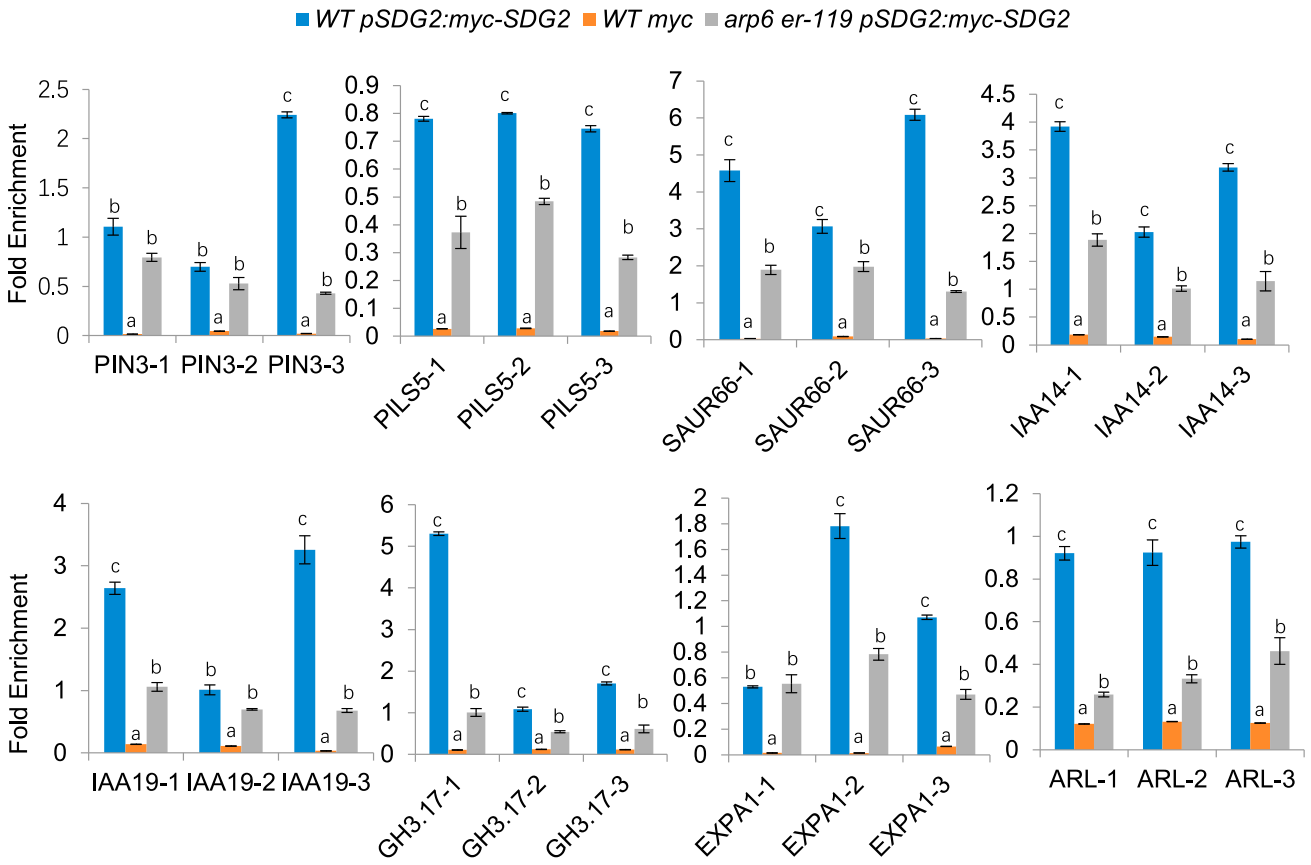

Figure 10. *SDG2* binds to auxin-related genes is involved in *SWR1-ER* signaling pathway

ChIP analysis for the enrichment of SDG2 at auxin-related genes in WT and *arp6 er-119* flower buds. Different letters above columns indicate significant difference at $p < 0.05$, as determined by one-way ANOVA.

development (Berr et al., 2010b). *SDG2* is involved in gamete mitotic cell cycle progression and pollen vegetative cell function (Pinon et al., 2017). Although *SDG2* had been reported to play a role in the regulation of vegetative growth and reproductive growth, including root development and gametophytic development (Yao et al., 2013), *SDG2*-mediated H3K4me3 deposition and function in inflorescence architecture is still poorly studied. SWR1 and H2A.Z cooperate with histone modifications to regulate gene expression on a genome-wide scale (Carter et al., 2018; Dai et al., 2018). H2A.Z associates with H3K4me3 at promoters to activate gene expression but represses the activities of enhancers by inhibiting H3K4me3 (Dai et al., 2018). In addition, the relationship between H2A.Z and H3K4me3 in plant-specific processes has also been revealed. For example, H2A.Z regulates vegetative phase change by facilitating the enrichment of H3K4me3 marks that promote the expression of the key microRNA genes *MIR156A* and *MIR156C* (Xu et al., 2018). In contrast, H2A.Z and H3K4me3 play antagonistic roles in regulating anthocyanin accumulation during plant responses to drought and high-light stress (Cai et al., 2019). In this study, we showed that *SDG2* is involved in the *SWR1-ER* signaling pathway, which has been reported to be involved in the regulation of inflorescence architecture (Cai et al., 2017, 2020). The *sdg2* single mutant had no obvious inflorescence phenotype, but the double mutants or triple mutants of *sdg2*, *arp6* and *er-119* had a compact inflorescence phenotype, which could be partially rescued by *pSDG2: myc-SDG2* expression. It is reported that the expression level and H3K4me3 level of *PRE1* was severely reduced in *sdg2* (Guo et al., 2010). Most importantly, our previous data showed that *PRE1* and its homologous, *PRE2*, *PRE5*, and *PRE6* are direct downstream components of the *ER* and *SWR1* complex, regulating inflorescence development (Cai et al., 2017). In addition, the more compact inflorescence and further reduced pedicels visible in *sdg2 pre-amiR* mutants indicated that *SDG2* genetically interacted with *PREs* in regulating inflorescence architecture. These results indicated that *SDG2* functions may act downstream of the *SWR1-ER* signaling pathway through affecting the expression of *PREs* in Arabidopsis inflorescence architecture or may act in parallel pathway with *SWR1-ER* signaling pathway regulating the Arabidopsis

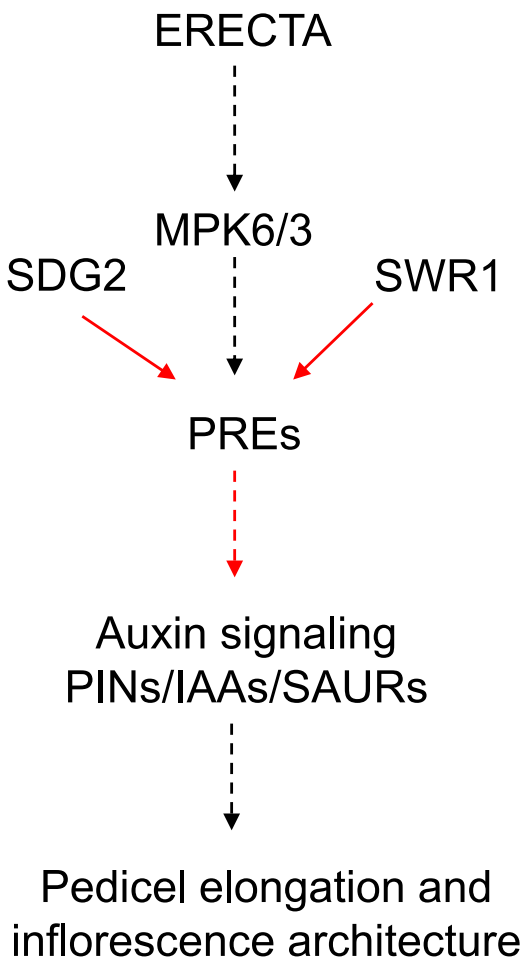

Figure 11. *SDG2* is involved in *SWR1-ER* signaling pathway in regulating inflorescence architecture

A diagram showing that *SDG2* is involved in *SWR1-ER* signaling pathway in regulating inflorescence architecture by activating the auxin signaling pathways. Red arrows indicate the activation relationships revealed by this study. Solid lines indicate direct binding, and dashed lines indicate indirect relationships.

inflorescence architecture (Figure 11). Our work, therefore, identified a new role for *SDG2* in the growth and development of Arabidopsis, as *SDG2* coordinates with *SWR1-ER* signaling pathway in regulating inflorescence architecture (Figure 11).

SDG2 regulates inflorescence architecture through potential roles of auxin

The regulation of plant inflorescence architecture is mediated by many factors, such as flowering time genes, *LSH1* family genes, and interaction between the auxin pathways (Teo et al., 2014). Auxin biosynthesis, transporter and response process are involved in floral meristem formation and inflorescence architecture; biosynthesis mediating by the *YUC* genes is essential for the formation of floral organs and vascular tissues (Cheng et al., 2006; Teo et al., 2014). Enhanced branching and decreased inflorescence branch angles were observed in *ful-7* mutants, *SMALL AUXIN UP-REGULATED RNA 10 (SAUR10)* was discovered that was repressed by MADS-domain factor *FRUITFULL (FUL)* in stems and inflorescence branches of Arabidopsis (Bemer et al., 2017). *BIK1* and *ER* play opposing roles in leaf morphogenesis and inflorescence architecture. *BIK1* is required to maintain an appropriate auxin response during leaf margin morphogenesis (Chen et al., 2019b). Our recent publication indicated that *HBI1* acted downstream of *SWR1* and *ER-MPK6* signaling pathway via binding to the promoter of brassinosteroid (BR) biosynthesis gene *CYP85A2* and auxin-related genes in regulating the inflorescence architecture, which revealed that auxin and BR signal regulating the inflorescence architecture synergistically (Cai et al., 2020). Here we showed that *SDG2* is involved in the *PREs*-controlled inflorescence architecture and may act in a parallel pathway to the *SWR1-ER* signaling pathway. Our recent work concluded that *PREs* function

downstream of *SWR1-ER* signaling pathway (Cai et al., 2017). Besides, previous research showed that *PRE1* was significantly down-regulated in *sdg2* (Guo et al., 2010). These results contribute that *SDG2* is required for the normal expression of *PREs* and may act upstream of *PREs*. Furthermore, the bHLH transcription factor genes *PRE1* were widely known as being involved in plant growth and development through the plant hormone pathway (Boeglin et al., 2016; Du et al., 2016; Guo et al., 2017). Our present work discovered that Pol II, H3K4me3, and H3K27me3 levels of auxin-related genes were altered in *SWR1-ER* and *SDG2* signaling pathways. We could infer that *SDG2* is associated with the *SWR1-ER* signaling pathway in regulating inflorescence architecture through mediating the expression of *PREs* and auxin-related genes. In addition, the *SWR1-ER* signaling pathway is required for the binding of *SDG2* to auxin-related genes. Taken together, *SDG2* was indicated that being involved in *SWR1-ER* signaling pathway through potential roles of auxin in regulating inflorescence architecture, one of the functions of *SDG2* underlying the development of inflorescence architecture was postulated.

Limitations of the study

In this study, we determined that SDG2 genetically interacts with the SWR1-ER signaling pathways in regulating inflorescence architecture. Transcriptome results showed that auxin may play potential roles in inflorescence growth mediated by SDG2 and SWR1-ER pathway. SWR1 and ER signaling are required to enrich H2A.Z histone variant and SDG2-mediated H3K4me3 histone modification at auxin related genes and H2A.Z histone variant enrichment was also regulated by SDG2. However, little is known about the roles of other epigenetic regulation marks or transcription factors in the control of inflorescence architecture. Additional studies are required to elucidate whether other epigenetics factors or transcription factors are involved in SWR1-ER signaling pathways in regulating inflorescence architecture.

STAR★METHODS

Detailed methods are provided in the online version of this paper and include the following:

- KEY RESOURCES TABLE
- RESOURCE AVAILABILITY
  - Lead contact
  - Materials availability
  - Data and code availability
- EXPERIMENTAL MODEL AND SUBJECT DETAILS
  - Plant materials and growth conditions
- METHOD DETAILS
  - Phenotype characterization and histological sections
  - Chromatin immunoprecipitation
  - Quantitative real-time RT-PCR
  - RNA-sequencing and data analysis
  - Western Blot
- QUANTIFICATION AND STATISTICAL ANALYSIS

SUPPLEMENTAL INFORMATION

Supplemental information can be found online at https://doi.org/10.1016/j.isci.2021.103236.

ACKNOWLEDGMENTS

We thank Dr. Xiaoyu Zhang, and Dr. Elena D. Shpak for providing the seeds. This work was supported by the National Natural Science Foundation of China (31970333 to Y.Q.; 31700279 to H.C.) and a Guangxi Distinguished Experts Fellowship to Y.Q and Science and Technology Major Project of Guangxi (GK2018-266-Z01). The funders had no role in the study design, data collection, and analysis, decision to publish, or preparation of the manuscript.

AUTHOR CONTRIBUTIONS

L.L. cloned the gene, generated the transgenic lines, and performed phenotypic and genetic analysis. M.C., Y.H., and J.Q. conducted ChIP analyses. W.Z., X.X., and F.C. performed qPCR experiments and analyzed the data. H.C. and Y.Q. revised the manuscript. H.C. and Y.Q. designed the research and wrote the manuscript.

DECLARATION OF INTERESTS

The authors declare no competing interests.

Received: May 2, 2021
Revised: August 30, 2021
Accepted: October 4, 2021
Published: November 19, 2021

REFERENCES

Alvarez-Venegas, R., and Avramova, Z. (2002). SET-domain proteins of the Su(var)3-9, E(z) and trithorax families. Gene *285*, 25–37.

Amasino, R.M., and Michaels, S.D. (2010). The timing of flowering. Plant Physiol. *154*, 516–520.

Aslam, M., Fakher, B., Jakada, B.H., Cao, S., and Qin, Y. (2019). SWR1 chromatin remodeling complex: a key transcriptional regulator in plants. Cells *8*, 1621.

Baumbusch, L.O., Thorstensen, T., Krauss, V., Fischer, A., Naumann, K., Assalkhou, R., Schulz, I., Reuter, G., and Aalen, R.B. (2001). The Arabidopsis thaliana genome contains at least 29 active genes encoding SET domain proteins that can be assigned to four evolutionarily conserved classes. Nucl. Acids Res. *29*, 4319–4333.

Bemer, M., van Mourik, H., Muino, J.M., Ferrandiz, C., Kaufmann, K., and Angenent, G.C. (2017). FRUITFULL controls SAUR10 expression and regulates Arabidopsis growth and architecture. J. Exp. Bot. *68*, 3391–3403.

Benlloch, R., Berbel, A., Serrano-Mislata, A., and Madueno, F. (2007). Floral initiation and inflorescence architecture: a comparative view. Ann. Bot. *100*, 659–676.

Berr, A., McCallum, E.J., Alioua, A., Heintz, D., Heitz, T., and Shen, W.H. (2010a). Arabidopsis histone methyltransferase SET DOMAIN GROUP8 mediates induction of the jasmonate/ethylene pathway genes in plant defense response to necrotrophic fungi. Plant Physiol. *154*, 1403–1414.

Berr, A., McCallum, E.J., Menard, R., Meyer, D., Fuchs, J., Dong, A., and Shen, W.H. (2010b). Arabidopsis SET DOMAIN GROUP2 is required for H3K4 trimethylation and is crucial for both sporophyte and gametophyte development. Plant Cell *22*, 3232–3248.

Berr, A., Xu, L., Gao, J., Cognat, V., Steinmetz, A., Dong, A., and Shen, W.H. (2009). SET DOMAIN GROUP25 encodes a histone methyltransferase and is involved in FLOWERING LOCUS C activation and repression of flowering. Plant Physiol. *151*, 1476–1485.

Boeglin, M., Fuglsang, A.T., Luu, D.T., Sentenac, H., Gaillard, I., and Cherel, I. (2016). Reduced expression of AtNUP62 nucleoporin gene affects auxin response in Arabidopsis. BMC Plant Biol. *16*, 2.

Bowler, C., Benvenuto, G., Laflamme, P., Molino, D., Probst, A.V., Tariq, M., and Paszkowski, J. (2004). Chromatin techniques for plant cells. Plant J. *39*, 776–789.

Cai, H., Chai, M., Chen, F., Huang, Y., Zhang, M., He, Q., Liu, L., Yan, M., and Qin, Y. (2020). HBI1 acts downstream of ERECTA and SWR1 in regulating inflorescence architecture through the activation of the brassinosteroid and auxin signaling pathways. New Phytol. *229*, 414–428.

Cai, H., Zhang, M., Chai, M., He, Q., Huang, X., Zhao, L., and Qin, Y. (2019). Epigenetic regulation of anthocyanin biosynthesis by an antagonistic interaction between H2A.Z. H3k4me3. New Phytol. *221*, 295–308.

Cai, H., Zhao, L., Wang, L., Zhang, M., Su, Z., Cheng, Y., Zhao, H., and Qin, Y. (2017). ERECTA signaling controls Arabidopsis inflorescence architecture through chromatin-mediated activation of PRE1 expression. New Phytol. *214*, 1579–1596.

Carter, B., Bishop, B., Ho, K.K., Huang, R., Jia, W., Zhang, H., Pascuzzi, P.E., Deal, R.B., and Ogas, J. (2018). The chromatin remodelers PKL and PIE1 act in an epigenetic pathway that determines H3K27me3 homeostasis in arabidopsis. Plant Cell *30*, 1337–1352.

Chen, M.S., Zhao, M.L., Wang, G.J., He, H.Y., Bai, X., Pan, B.Z., Fu, Q.T., Tao, Y.B., Tang, M.Y., Martinez-Herrera, J., et al. (2019a). Transcriptome analysis of two inflorescence branching mutants reveals cytokinin is an important regulator in controlling inflorescence architecture in the woody plant Jatropha curcas. BMC Plant Biol. *19*, 468.

Chen, S., Liu, J., Liu, Y., Chen, L., Sun, T., Yao, N., Wang, H.B., and Liu, B. (2019b). BIK1 and ERECTA play opposing roles in both leaf and inflorescence development in arabidopsis. Front Plant Sci. *10*, 1480.

Cheng, Y., Dai, X., and Zhao, Y. (2006). Auxin biosynthesis by the YUCCA flavin monooxygenases controls the formation of floral organs and vascular tissues in Arabidopsis. Genes Dev. *20*, 1790–1799.

Choi, K., Kim, S., Kim, S.Y., Kim, M., Hyun, Y., Lee, H., Choe, S., Kim, S.G., Michaels, S., and Lee, I. (2005). SUPPRESSOR OF FRIGIDA3 encodes a nuclear ACTIN-RELATED PROTEIN6 required for floral repression in Arabidopsis. Plant Cell *17*, 2647–2660.

Cui, L., Zheng, F., Wang, J., Zhang, C., Xiao, F., Ye, J., Li, C., Ye, Z., and Zhang, J. (2020). miR156a-targeted SBP-Box transcription factor SlSPL13 regulates inflorescence morphogenesis by directly activating SFT in tomato. Plant Biotechnol. J. *18*, 1670–1682.

Dai, X., Bai, Y., Zhao, L., Dou, X., Liu, Y., Wang, L., Li, Y., Li, W., Hui, Y., Huang, X., et al. (2018). H2A.Z represses gene expression by modulating promoter nucleosome structure and enhancer histone modifications in arabidopsis. Mol. Plant *11*, 635.

Du, J., Gao, Y., Zhan, Y., Zhang, S., Wu, Y., Xiao, Y., Zou, B., He, K., Gou, X., Li, G., et al. (2016). Nucleocytoplasmic trafficking is essential for BAK1- and BKK1-mediated cell-death control. Plant J. *85*, 520–531.

Fernandez-Nohales, P., Domenech, M.J., Martinez de Alba, A.E., Micol, J.L., Ponce, M.R., and Madueno, F. (2014). AGO1 controls arabidopsis inflorescence architecture possibly by regulating TFL1 expression. Ann. Bot. *114*, 1471–1481.

Guo, C., Xu, Y., Shi, M., Lai, Y., Wu, X., Wang, H., Zhu, Z., Poethig, R.S., and Wu, G. (2017). Repression of miR156 by miR159 regulates the timing of the juvenile-to-adult transition in arabidopsis. Plant Cell *29*, 1293–1304.

Guo, L., Yu, Y., Law, J.A., and Zhang, X. (2010). SET DOMAIN GROUP2 is the major histone H3 lysine [corrected] 4 trimethyltransferase in Arabidopsis. Proc. Natl. Acad. Sci. U S A *107*, 18557–18562.

Hu, G., Cui, K., Northrup, D., Liu, C., Wang, C., Tang, Q., Ge, K., Levens, D., Crane-Robinson, C., and Zhao, K. (2013). H2A.Z facilitates access of active and repressive complexes to chromatin in embryonic stem cell self-renewal and differentiation. Cell Stem Cell *12*, 180–192.

Huijser, P., and Schmid, M. (2011). The control of developmental phase transitions in plants. Development *138*, 4117–4129.

Jiang, P., Wang, S., Ikram, A.U., Xu, Z., Jiang, H., Cheng, B., and Ding, Y. (2018). SDG721 and SDG705 are required for rice growth. J. Integr. Plant Biol. *60*, 530–535.

Kumar, S.V. (2018). H2A.Z at the core of transcriptional regulation in plants. Mol. Plant *11*, 1112–1114.

Li, L., Liu, B., Wapinski, O.L., Tsai, M.C., Qu, K., Zhang, J., Carlson, J.C., Lin, M., Fang, F., Gupta, R.A., et al. (2013). Targeted disruption of Hotair leads to homeotic transformation and gene derepression. Cell Rep. *5*, 3–12.

Li, Y., Li, X., Fu, D., and Wu, C. (2018). Panicle Morphology Mutant 1 (PMM1) determines the inflorescence architecture of rice by controlling brassinosteroid biosynthesis. BMC Plant Biol. *18*, 348.

Liu, B., Wei, G., Shi, J., Jin, J., Shen, T., Ni, T., Shen, W.H., Yu, Y., and Dong, A. (2016). SET DOMAIN GROUP 708, a histone H3 lysine 36-specific methyltransferase, controls flowering

time in rice (Oryza sativa). New Phytol. *210*, 577–588.

Liu, K., Yu, Y., Dong, A., and Shen, W.H. (2017). SET DOMAIN GROUP701 encodes a H3K4-methytransferase and regulates multiple key processes of rice plant development. New Phytol. *215*, 609–623.

Meng, X., Wang, H., He, Y., Liu, Y., Walker, J.C., Torii, K.U., and Zhang, S. (2012). A MAPK cascade downstream of ERECTA receptor-like protein kinase regulates Arabidopsis inflorescence architecture by promoting localized cell proliferation. Plant Cell *24*, 4948–4960.

Mizuguchi, G., Shen, X., Landry, J., Wu, W.H., Sen, S., and Wu, C. (2004). ATP-driven exchange of histone H2AZ variant catalyzed by SWR1 chromatin remodeling complex. Science *303*, 343–348.

Oh, E., Zhu, J.Y., and Wang, Z.Y. (2012). Interaction between BZR1 and PIF4 integrates brassinosteroid and environmental responses. Nat. Cell Biol. *14*, 802–809.

Pinon, V., Yao, X., Dong, A., and Shen, W.H. (2017). SDG2-mediated H3K4me3 is crucial for chromatin condensation and mitotic division during male gametogenesis in Arabidopsis. Plant Physiol. *174*, 1205–1215.

Prusinkiewicz, P., Erasmus, Y., Lane, B., Harder, L.D., and Coen, E. (2007). Evolution and development of inflorescence architectures. Science *316*, 1452–1456.

Shin, K., Lee, I., Kim, E., Park, S.K., Soh, M.S., and Lee, S. (2019). PACLOBUTRAZOL-RESISTANCE gene family regulates floral organ growth with unequal genetic redundancy in *Arabidopsis thaliana*. Int. J. Mol. Sci. *20*, 869.

Smyth, D.R., Bowman, J.L., and Meyerowitz, E.M. (1990). Early flower development in Arabidopsis. Plant Cell *2*, 755–767.

Springer, N.M., Napoli, C.A., Selinger, D.A., Pandey, R., Cone, K.C., Chandler, V.L., Kaeppler, H.F., and Kaeppler, S.M. (2003). Comparative analysis of SET domain proteins in maize and Arabidopsis reveals multiple duplications preceding the divergence of monocots and dicots. Plant Physiol. *132*, 907–925.

Teo, Z.W., Song, S., Wang, Y.Q., Liu, J., and Yu, H. (2014). New insights into the regulation of inflorescence architecture. Trends Plant Sci. *19*, 158–165.

Wu, G., and Poethig, R.S. (2006). Temporal regulation of shoot development in *Arabidopsis thaliana* by miR156 and its target SPL3. Development *133*, 3539–3547.

Xu, M., Hu, T., Zhao, J., Park, M.Y., Earley, K.W., Wu, G., Yang, L., and Poethig, R.S. (2016). Developmental functions of miR156-Regulated SQUAMOSA PROMOTER BINDING PROTEIN-LIKE (SPL) genes in *Arabidopsis thaliana*. PLoS Genet. *12*, e1006263.

Xu, M., Leichty, A.R., Hu, T., and Poethig, R.S. (2018). H2A.Z promotes the transcription of MIR156A and MIR156C in Arabidopsis by facilitating the deposition of H3K4me3. Development *145*, dev152868.

Yao, X., Feng, H., Yu, Y., Dong, A., and Shen, W.H. (2013). SDG2-mediated H3K4 methylation is required for proper Arabidopsis root growth and development. PLoS One *8*, e56537.

Yun, J.Y., Tamada, Y., Kang, Y.E., and Amasino, R.M. (2012). Arabidopsis trithorax-related3/SET domain GROUP2 is required for the winter-annual habit of Arabidopsis thaliana. Plant Cell Physiol. *53*, 834–846.

Zhang, X., Zou, Z., Zhang, J., Zhang, Y., Han, Q., Hu, T., Xu, X., Liu, H., Li, H., and Ye, Z. (2011). Over-expression of sly-miR156a in tomato results in multiple vegetative and reproductive trait alterations and partial phenocopy of the sft mutant. FEBS Lett. *585*, 435–439.

Zhao, L., He, J., Cai, H., Lin, H., Li, Y., Liu, R., Yang, Z., and Qin, Y. (2014). Comparative expression profiling reveals gene functions in female meiosis and gametophyte development in Arabidopsis. Plant J. *80*, 615–628.

Zhao, Z., and Shen, W.H. (2004). Plants contain a high number of proteins showing sequence similarity to the animal SUV39H family of histone methyltransferases. Ann. N Y Acad. Sci. *1030*, 661–669.

Zhao, Z., Yu, Y., Meyer, D., Wu, C., and Shen, W.H. (2005). Prevention of early flowering by expression of FLOWERING LOCUS C requires methylation of histone H3 K36. Nat. Cell Biol. *7*, 1256–1260.

Zhou, H., Liu, Y., Liang, Y., Zhou, D., Li, S., Lin, S., Dong, H., and Huang, L. (2020). The function of histone lysine methylation related SET domain group proteins in plants. Protein Sci. *29*, 1120–1137.

STAR★METHODS

KEY RESOURCES TABLE

REAGENT or RESOURCE	SOURCE	IDENTIFIER
Experimental models: Organisms		
Arabidopsis: *arp6*	(Cai et al., 2017)	N/A
Arabidopsis: *er-119*	(Cai et al., 2017)	N/A
Arabidopsis: *sdg2*	This paper	N/A
Arabidopsis: *arp6 er-119*	(Cai et al., 2017)	N/A
Arabidopsis: *arp6 sdg2*	This paper	N/A
Arabidopsis: *er-119 sdg2*	This paper	N/A
Arabidopsis: *arp6 er-119 sdg2*	This paper	N/A
Arabidopsis: *pSDG2:myc-SDG2*	(Guo et al., 2010)	N/A
Arabidopsis: *pre-amiR*	(Cai et al., 2017)	N/A
Arabidopsis: *sdg2pre-amiR*	This paper	N/A
Antibodies		
Rabbit monoclonal anti-MYC	This paper	Abcam ab9132
H2A.Z polyclonal antibody	R. Deal' Lab	N/A
H3K27me3 polyclonal antibody	This paper	Millipore, 07-449
H3K4me3 polyclonal antibody	This paper	Millipore, 07-473
Pol II monoclonal antibody	This paper	Abcam ab817
Chemicals, peptides, and recombinant proteins		
Total RNA Kit II	Omega	R6934-01
Qiagen RNeasy kit	Qiagen	74106

RESOURCE AVAILABILITY

Lead contact

Further information and requests for resources and reagents should be directed to and will be fulfilled by the lead contact, Hanyang Cai (caihanyang123@163.com).

Materials availability

This study did not generate new unique reagents.

Data and code availability

- The original RNA-seq data is available at European Nucleotide Archive (ENA) under accession number PRJEB47720.
- No original code was produced in this study.
- Any additional information required to reanalyze the data reported in this paper is available from the lead contact upon request.

EXPERIMENTAL MODEL AND SUBJECT DETAILS

Plant materials and growth conditions

The *Arabidopsis thaliana* Columbia (Col-0) ecotype was used in this study. The other Arabidopsis mutant lines were described as follows: *arp6* (*Garlic_599_G03*), *sdg2* (*SALK_021008*), *pSDG2:myc-SDG2* (Guo et al., 2010), *pre-amiR* (Oh et al., 2012), *er-119* (Cai et al., 2017). After vernalizing at 4°C for 36-48 hours, all the described wild-type and mutant seeds were planted and grown in soil at 22°C under 16 h-light/8 h-dark photoperiod conditions.

METHOD DETAILS

Phenotype characterization and histological sections

To analysis the phenotype of inflorescence, the inflorescence and signal flower were placed on 1/2 MS medium, followed by observation under a Lecia (M205 FA) microscope. Fixing of Pedicel tissue sample was performed as described previously (Cai et al., 2020) and dehydrated through a graded series of ethanol (30, 50, 70, 80, 90, 95 and 100%). The dehydrated sample was infiltrated with Eponate 812 resin (TED Pella, Inc.), followed by embedding with Eponate 812 resin (TED Pella, Inc.) and polymerization process in an incubator 40℃for 12h, 60°C for 18-36h. The Leica (RM2255) microtome was used to cut 1.5-2μm sections, followed by observation under Olympus (BX63) microscope. The number of cells in a middle longitudinal cortex row was counted, and this number was used to calculate the total number and average length of cells in the cortex row of each pedicel. The number of cells was counted using 15–20 sectioned pedicels for each genotype. Cell length was measured directly on the photographic images of plastic sections (Cai et al., 2017).

Chromatin immunoprecipitation

For each chromatin immunoprecipitation (ChIP) experiment, 1.5 g of floral bud tissue at stages 11–14 was used. Floral buds were formaldehyde cross-linked as described (Bowler et al., 2004). Cross linked chromatin was fragmented with 0.2 units of micrococcal nuclease (Sigma) in 1 ml of MNase digestion buffer (10 mM Tris-HCl (pH 8.0), 50 mM NaCl, 1 mM-mercaptoethanol, 0.1% NP40, 1 mM CaCl2, and 1 9 protease inhibitor cocktail, Roche). Digestion was stopped using 5 mM EDTA. ChIP was performed using an H2A.Z polyclonal antibody (from R. Deal, Emory University), or polyclonal antibody against H3K27me3 (Millipore, 07- 449), a polyclonal antibody against H3K4me3 (Millipore, 07-473), or a monoclonal antibody against the RNA polymerase II CTD repeat YSPTSPS (Abcam ab817). Relative enrichment of associated DNA fragments was analyzed by qPCR. All oligonucleotide sequences used in the ChIP experiments are given in Table S1. Each ChIP experiment was repeated three times, and the data represent the average of three biological replicates (Cai et al., 2017, 2020).

Quantitative real-time RT-PCR

RNA was isolated from pedicel tissues of developing flowers at stages 11–14. Total RNA was extracted using the Omega Total RNA Kit II and reverse transcribed into cDNA using the TransScript All-in-One transcription kit. For quantitative RT-PCR, 50 ng cDNA was used to detect the transcript levels of marker genes, and HK2 was used as an internal control. Quantitative real-time (qRT)-PCR was performed with specific primers (Table S1) on the Bio-Rad real-time PCR system. Data were analyzed and presented as the normalized relative expression level ($2^{\Delta\Delta CT}$) of the respective genes in different samples (Cai et al., 2017).

RNA-sequencing and data analysis

RNA was extracted from inflorescence with flower buds younger than stage 14 (Smyth et al., 1990) using the Qiagen RNeasy kit. We were using the Qiagen RNeasy kit. One microgram of RNA from each sample for three independent biological replicates was used for Illumina Sequencing, performed as previously described (Zhao et al., 2014). We performed data analysis as previously described and the *Arabidopsis thaliana* genome from TAIR 10 as reference (Cai et al., 2020).

Western Blot

Proteins were separated by electrophoresis in 15% SDS-polyacrylamide gels and then transferred to PVDF membrane in CAPS/methanol buffer. Primary antibodies specific for anti-H3K4me3 (Millipore, 07-473).

QUANTIFICATION AND STATISTICAL ANALYSIS

All t-test analysis was conducted using Excel, and the ANOVA analysis was conducted using SPSS software. To determine statistical significance, we employed independent t-tests with two-tail distribution between two groups and one-way ANOVA Turkey's test among various genotypes. A value of $p < 0.05$ was considered to be statistically significant.